Confinement of surface spinners in liquid metamaterials

Jean-Baptiste Gorce[a,1], Hua Xia[a], Nicolas Francois[a], Horst Punzmann[a], Gregory Falkovich[b,c], and Michael Shats[a,1]

[a]Research School of Physics, The Australian National University, Canberra, ACT 2601, Australia; [b]Department of Physics, Weizmann Institute of Science, Rehovot 76100, Israel; and [c]Photonics Center, Novosibirsk State University, Novosibirsk 630090, Russia

Edited by Igor Aronson, Pennsylvania State University, University Park, PA, and accepted by Editorial Board Member Peter J. Rossky November 4, 2019 (received for review July 26, 2019)

We show that rotating particles at the liquid–gas interface can be efficiently manipulated using the surface-wave analogue of optical lattices. Two orthogonal standing waves generate surface flows of counter-rotating half-wavelength unit cells, the liquid interface metamaterial, whose geometry is controlled by the wave phase shift. Here we demonstrate that by placing active magnetic spinners inside such metamaterials, one makes a powerful tool which allows manipulation and self-assembly of spinners, turning them into vehicles capable of transporting matter and information between autonomous metamaterial unit cells. We discuss forces acting on a spinner carried by a nonuniform flow and show how the forces confine spinners to orbit inside the same-sign vortex cells of the wave-driven flow. Reversing the spin, we move the spinner into an adjacent cell. By changing the spinning frequency or the wave amplitude, one can precisely control the spinner orbit. Multiple spinners within a unit cell self-organize into stable patterns, e.g., triangles or squares, orbiting around the center of the cell. Spinners having different frequencies can also be confined, such that the higher-frequency spinner occupies the inner orbit and the lower-frequency one circles on the outer orbit, while the orbital motions of both spinners are synchronized.

active spinners | fluid vortex lattice | wave control | water wave

Manipulation of microparticles at liquid–gas interfaces is a desired tool in many applications including self-assembly into patterns and structures (1–8). Active particles on the liquid surface, such as magnetic spinners, attracted considerable attention because of their ability to self-assemble when placed within a potential well (1). That self-assembly in a magnetic trap revealed a repulsive force between spinners, which appears due to a hydrodynamic (lift) force, proportional to the rotation frequency and acting on each particle (1–3).

Recent advances in confinement and manipulation of microparticles and ultracold atoms using optical waves (9, 10) inspired new ideas related to the control of particles at liquid–gas interfaces using the so-called liquid interface metamaterials or dynamic periodic patterns on the liquid surface driven by crossed surface waves (11). Optical lattices and liquid metamaterials have a number of similarities, although owing to fundamental differences in the nature of electromagnetic and hydrodynamic surface waves, the mechanisms of wave–particle interaction are very different. In liquid metamaterials, the wave angular momentum is transferred to passive fluid particles guiding them along complex periodic orbits (11). For microparticles and cold atoms, electromagnetic waves generate dipole forces due to the polarization of particles by the waves. The trapping location in an optical wave (e.g., nodes or antinodes) is determined by the polarizability and, in ultracold atom physics, by the tuning of the wave frequency relative to the frequency of the atomic resonance (12). However, the trapping of micro- and nanoparticles in optical manipulation experiments is also affected by hydrodynamics forces. For example, spinning microparticles in circularly polarized laser beams are affected by the Magnus force, a phenomenon well known in ball games (13). The comparison between waves in fluids and electromagnetic waves in optics can be productive if the analogies are carefully mapped across, as for example in the case of the Faraday waves and phase-conjugate mirrors (14).

Passive or tracer particles on the fluid surface can also be manipulated by dynamic structures, for example using wave-based templates capable of assembling microparticles in reconfigurable and biocompatible ways (15, 16). Surface waves are a powerful tool which can be used to control particles at the liquid surface. Liquid interface metamaterials (11) resemble vortex lattices which are found in a variety of contexts in physical and biological systems, such as bacterial suspensions (17), collectively moving microtubules (18), sperm cells (19), or electromagnetically driven vortex lattices in electrolytes (20–22). Such flows are made of periodic patterns of vortices. Each vortex is a set of nested smooth closed-particle orbits. The liquid metamaterials, however, differ substantially from the above examples. Closed orbits of the fluid particles are not circles, but rather they are curved trochoids resulting from a drift motion similar to the Stokes drift (23), as described in the next section. Crossed standing surface waves generate a matrix of cellular flows whose geometry depends on the relative phase shift between 2 orthogonal waves. Surface waves show features similar to polarized electromagnetic waves (11, 24): 1) Near nodal points fluid particles trace straight lines, ellipses, or circles depending on the phase shift, and 2) orthogonal waves that are phase shifted by 90° produce the unit cells of the metamaterial. These unit cells are well isolated from each other, in contrast to the traditional vortex lattices, such as the electromagnetically driven vortices

Significance

The ability to control and separate individual active particles in fluid layers is a challenge in biological and engineering contexts as well as a basic problem of controlled self-assembly. Here we place spinners in a wave-driven matrix of vortices, akin to optical lattices. The results offer a method of manipulating spinning particles within a wave-produced flow. Spinners can be confined on stable orbits, trapped inside, or released from the liquid metamaterial cells without solid boundaries and can be used to carry biological or chemical agents within the vortex lattice.

Author contributions: J.-B.G., H.X., N.F., H.P., and M.S. designed research; J.-B.G., H.P., G.F., and M.S. performed research; J.-B.G., H.X., N.F., and G.F. analyzed data; and J.-B.G., G.F., and M.S. wrote the paper.

The authors declare no competing interest.

This article is a PNAS Direct Submission. I.A. is a guest editor invited by the Editorial Board.

Data deposition: The data used for Fig. 2B is available at https://figshare.com/s/6d92ceab338607923f1e. Custom Matlab code to track the spinner motion is available at https://figshare.com/s/641b204f501f0b8c5c16.

[1]To whom correspondence may be addressed. Email: Michael.Shats@anu.edu.au or Jean-Baptiste.Gorce@anu.edu.au.

This article contains supporting information online at https://www.pnas.org/lookup/suppl/doi:10.1073/pnas.1912905116/-/DCSupplemental.

First published December 4, 2019.

in layers of electrolytes (22) and the Faraday wave-driven flows, where the vortices strongly interact, forming 2-dimensional (2D) turbulence (25, 26). For this reason we refer to our flow as a liquid-interface metamaterial to distinguish it from the classical vortex lattices.

Floating particles can be externally energized; for instance, floating magnetic disks spin around their centers in a rotating magnetic field (1). Here we demonstrate that such spinning disks can be efficiently trapped within the unit cells of a liquid metamaterial. Such trapping allows precise control of the orbits, the selectivity of a confining unit cell, and self-assembly of multiple spinners within a single unit cell. The presence of the spinners does not destroy or significantly disturb the lattice. Stationary orbits can be precisely controlled by adjusting the spinner frequency, as well as the frequency and the amplitude of the waves. The disks are trapped only within the cells having the same rotation direction as the spinning disk. If the rotation directions of the cell and of the disk are opposite, the disks are repelled into the adjacent unit cell. Multiple spinners (up to 4 spinners of the same frequency) can share stationary orbits whose radii depend on the number of orbiting spinners. Spinners with different angular frequencies occupy stationary orbits with different radii.

We thus suggest that particles with an externally controlled spin are peculiarly suitable for interacting with polarized surface waves of the liquid metamaterial, akin to the interaction between electromagnetic waves and polarized micro/nanoparticles and ultracold atoms. That allows methods of manipulation and confinement of microscopic particles energized by external fields at the fluid interfaces, which are needed in studies of ensembles of active agents.

Surface Flows Due to 2 Orthogonal Standing Waves

Two orthogonal standing surface waves with a frequency ω, a wavenumber $k=2\pi/\lambda$, phase shifted by ϕ on a liquid of depth d have the velocity potential $\Phi=(u/k)\cosh[k(z+d)][\sin(\omega t)\cos(kx)+\sin(\omega t+\phi)\cos(ky)]$. When $\phi=\pi/2$, it generates a pattern of surface elevation in which an antinode (a peak/trough location) rotates about a local nodal point (a point of constant in time surface elevation) (11). Such a rotation leads to the momentum transfer from the wave to the fluid particles, forcing them to proceed along closed trochoidal orbits (made by the loop motion and the drift), such as those seen in Fig. 1*A*. Let us give a brief theoretical description of the period-averaged fluid flow within the $\lambda/2\times\lambda/2$ unit cell. We solve the Lagrangian equation on the coordinate of a fluid particle, $d\mathbf{R}/dt=\nabla\Phi(\mathbf{R},t)=\mathbf{v}(\mathbf{R})\sin(\omega t)+\mathbf{u}(\mathbf{R})\sin(\omega t+\phi)$, perturbatively in ku/ω. It gives the loop motion in the first order. In the second order, we obtain the net Lagrangian drift velocity averaged over the period (27): $\boldsymbol{w}=\sin\phi\,[(\boldsymbol{u})\boldsymbol{v}-(\boldsymbol{v})\boldsymbol{u}]/2\omega$. It is the product of the geometrical phase determined by the phase shift and the commutator of the velocity fields of 2 waves. One may think that it is zero, since the 2D commutator is zero, but the whole 3-dimensional (3D) commutator is not: $w_x=u_z\nabla_z v_x=(ku^2/\omega)\sin\phi\cos(kx)\sin(ky)$, $w_y=-v_z\nabla_z u_y=(ku^2/\omega)\sin\phi\sin(kx)\cos(ky)$. Indeed, the Lagrangian trajectories are 3D, as shown in ref. 11. The clockwise rotation during one wave period (at $\phi=\pi/2$) corresponds to the clockwise drift, as seen in Fig. 1*A*, *Top Right* and *Bottom Left* unit cells. Such velocities correspond to the stream function given by

$$\Psi=\left(u^2/\omega\right)\cos(kx)\cos(ky), \qquad [1]$$

where $u=A\omega$ and A is the wave amplitude. Near the nodal point, the stream function describes a solid-body circular rotation (drift) of fluid; the drift velocity increases linearly with the distance from the node. The basic features of the Lagrangian trajectories can be seen in Fig. 1*A*: The relative drift (proportional to the shift of a tracer during one wave period) increases with the distance from the node. Fig. 1*B* shows a measured radial profile of the velocity of azimuthal drift (tangential to the drift orbit) of the tracer particles. Indeed, the fluid in the inner part of the unit cell moves as a solid body, while closer to the cell boundary the drift velocity saturates.

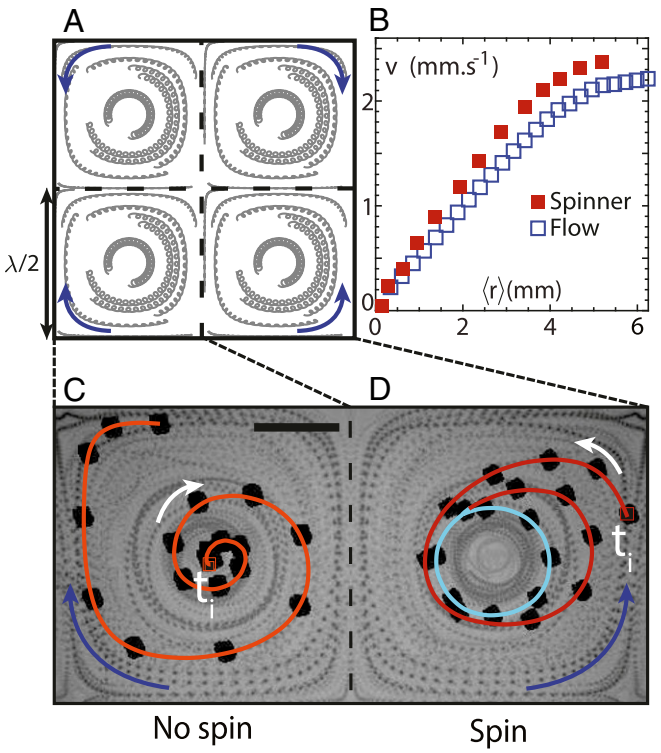

Fig. 1. Confinement of tracers, inertial particles, and spinners on the surface of the wave-driven vortex lattice. The wave frequency is 9.4 Hz and the wave's amplitude is 0.7 mm. (*A*) Horizontal projection of the trajectories of the tracers in 2 orthogonal standing surface waves, phase shifted by $\pi/2$. An area $\lambda\times\lambda$ (where λ is the wavelength) accommodates 4 unit cells confining surface tracers. The center of each cell is a nodal (zero) point of surface elevation. The Stokes-like drift of the fluid particles proceeds along closed orbits in opposite directions in the adjacent cells, as indicated by blue arrows. (*B*) Radial profiles of the azimuthal velocity of the tracers inside the unit cell (open blue squares) and of the 1-mm diameter spinners occupying stationary orbits (solid red squares). (*C*) A trajectory of an inertial (1-mm diameter) passive particle shows the existence of the radially outward force pushing the particle from the cell center into the separatrix region along the clockwise spiral trajectory. (*D*) The same particle as in *C* is now energized using an external rotating magnetic field. When it acquires the spin angular momentum, a radially inward force pushes it along the anticlockwise spiral trajectory onto a finite-size inner orbit. White arrows indicate the spiral direction; blue arrows indicate the direction of the cell fluid drift. (Scale bar in *C*, 4.5 mm.)

Trapping a Single Spinner in the Fluid Vortex Lattice

The tracer particles are confined within the unit cells of the liquid metamaterials as they execute closed trochoidal trajectories seen in Fig. 1*A*. They are guided by the rotating wave phase as described above. However, for the finite-size particles of slightly higher density, inertial effects become important and a 1-mm diameter floating disk spirals out from the center of the cell into the separatrix region, Fig. 1*C* (*Materials and Methods*). The outward force acting on the inertial particles inside the unit cells is a centrifugal force resulting from the curvilinear drift of the disk. In the inner core of the cell, the spiral shows a constant angular frequency and constant radially outward force. This force decreases at the unit cell boundary. Nonspinning disks tend to

stay within the separatrix region without being confined to any particular cell. The centrifugal acceleration $a_c \propto V_\theta^2/r_c$ depends on the radius of curvature of the orbit r_c. This radius of curvature changes as a function of the distance from the center of the cell, as seen in Fig. 1*A*: Inner orbits are circular, while the outer orbits and the separatrix are squares, where $r_c \to \infty$. At the square cell boundary the centrifugal force vanishes, except for the corners.

When the magnetic disk is energized and forced to spin at a frequency f_s, it spirals from the separatrix toward the center of the unit cell of the metamaterial. The disk acquires a velocity relative to the surrounding fluid (Fig. 1 *B* and *D*), which results from its interaction with the ambient flow (28) as discussed below. The disk traces a closed orbit whose radius depends on the spinner frequency f_s as illustrated in Fig. 2 *A* and *B*. The inward force pushing the spinner to the cell center balances the centrifugal outward force, resulting in the spinner occupying a stationary orbit, such as those shown in Fig. 2*A*. The higher the spinner frequency is, the smaller the spinner orbit radius $\langle r_s \rangle$. This is illustrated in Fig. 2*B*, suggesting that the inward force increases with the increase in f_s. Since the orbits within a unit cell are generally not circular, the average "radius" of the spinner orbit is defined as

$$\langle r_s \rangle = \left\langle \sqrt{(x(t)-x_0)^2 + (y(t)-y_0)^2} \right\rangle_t , \qquad [2]$$

where $(x(t),\ y(t))$ is the spinner's position and (x_0, y_0) is the position of the center of the unit cell; the angular brackets denote the time averaging. On the stationary orbit, the spinner propagates with the velocity which is slightly higher than the fluid drift velocity, as seen in Fig. 1*B*, suggesting that the spinner moves relative to the fluid.

The inward force changes sign when the spinning direction changes, as shown in Fig. 2 *C* and *D*. If the direction of the spin does not coincide with the direction of the fluid (wave-driven) drift, the spinner is pushed out of the unit cell into one of the adjacent cells whose polarization coincides with that of the spinner, as shown in Fig. 2*D*. Thus, for a single spinner within a unit cell, by changing the spinner direction one can select the trapping cell and can also change the exact size of the orbit by changing the spinner frequency for a given amplitude of the standing waves.

The amplitude of the crossed standing waves affects the wave-driven drift velocity of fluid (11) and its angular frequency Ω. The higher the wave amplitude is, the larger the Ω, as shown in Fig. 2*E*. The increase in the wave amplitude A_w leads to the increase in the outward centrifugal force. For a given spinner frequency, the radius of the stationary orbit $\langle r_s \rangle$, determined by the balance between this force and the spin-related inward force, increases, as illustrated in Fig. 2*F*. This result means that the outward centrifugal force increases faster with the increase in the wave amplitude than the inward force (discussed below).

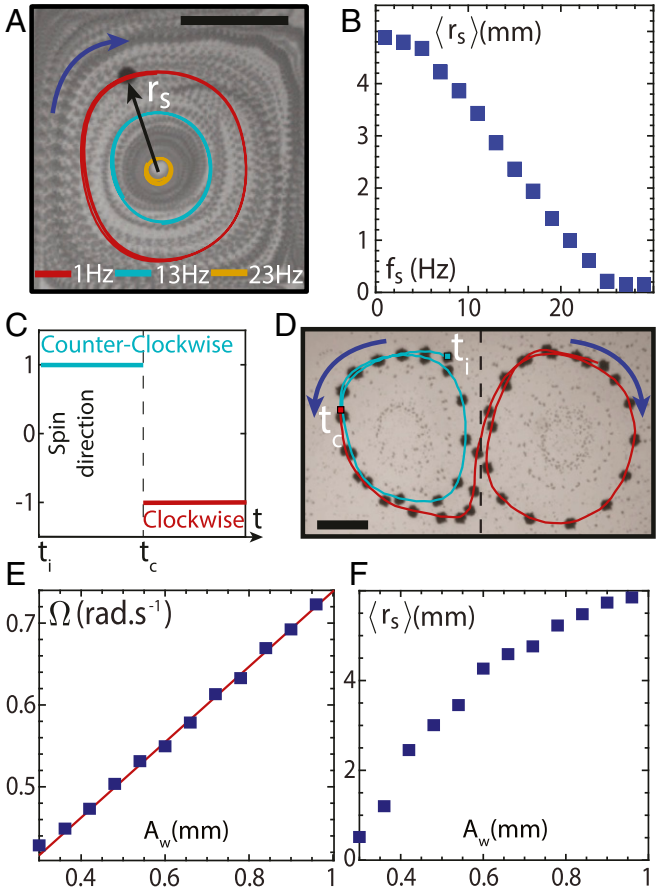

Fig. 2. Single spinner within a unit cell. (*A*–*D*) The wave frequency is 9.4 Hz and the wave's amplitude is 0.7 mm. (*A*) The orbit radius within the cell at a given wave frequency f_w can be controlled by changing the spinner frequency f_s (red, cyan, and yellow orbits correspond to $f_s = 1, 13, 23$ Hz, respectively) (Movie S1). (*B*) The increase in f_s (at constant wave amplitude and frequency $f_w = 9.4$ Hz) leads to a gradual reduction in the spinner orbit radius (blue squares). (*C*) The spin direction is switched by changing the rotation direction of the external magnetic field. (*D*) A spinner ($f_s = 15$ Hz) occupies a stationary orbit in the left unit cell (light blue trajectory). After switching the spin direction at $t = t_c$ (from corotation with the cell flow to counter rotation) the spinner moves out into the adjacent cell whose flow direction coincides with its new spin (red trajectory). (*E*) The angular velocity of the orbital motion linearly increases with the wave amplitude A_w at constant f_s. (*F*) The radius of the stationary orbit at constant f_s increases with the wave amplitude. (Scale bars in *A* and *D*, 4.5 mm.)

Trapping Multiple Spinners

Now we consider trapping of several spinners (of 1-mm diameter) within the liquid metamaterials. Fig. 3 shows trapping of 2, 3, and 4 spinners within a single unit cell. Two spinners orbit around the cell center, staying on the orbit diameter (Fig. 3*A*); 3 spinners form a rotating triangle (Fig. 3*B*); while up to 4 spinners form a rotating square (Fig. 3*C*). The orbiting velocity has the same direction as the underlying fluid drift, but the spinners move faster than the fluid.

The orbital radii increase with the number of spinners, as shown in Fig. 3*D*. A single spinner of the same frequency is trapped near the center of the unit cell. Remarkably, as the spinners' frequency is increased, the orbit radii only marginally change. This suggests that the trapping (inward) force scales similarly.

The orbital velocity of the clusters exceeds the wave-driven fluid velocity, similar to the single-spinner case (Fig. 1*B*). Fig. 4*B* shows the orbital velocity of a pair of spinners relative to the fluid U_{rel} as a function of the spinner frequency. The order of magnitude of the relative velocities of a single spinner and of the multispinner cluster is comparable. However, the single-spinner velocity is roughly independent of f_s (Fig. 4*A*), while for multiple spinners the relative orbital velocity U_{rel} increases with the increase in the spinner frequency (Fig. 4*B*). The repulsion force between the spinners and the confining force scale very similarly with the spinner frequency. The orbit radius only slightly increases with f_s. The orbit radius of the 4 spinners ($\sim$6 mm) is close in our configuration to the size of the unit cell ($\sim$6.5 mm). Any increase in the number of spinners above 4 makes the configuration unstable since it becomes larger than the cell size. An increase in the f_s above 20 Hz in the 4-spinner configuration pushes the collective orbit outside the unit cell and destroys the confinement.

One can create a configuration when 2 spinners of the same frequency, but with opposite spin directions, occupy 2 adjacent unit cells (*Materials and Methods*), as shown in Fig. 3*E*. In this case, they are stably confined. In this example spinners with relatively high spin frequencies of $f_s = 20$ Hz are trapped, each within its own unit cell; however, the separatrix between the unit cells is not perturbed. This result highlights the robustness of the wave-driven vortex lattice: Even fast-rotating spinners do not cause the merger of the neighboring "vortices."

Finally, we illustrate the confinement within a single unit cell of 2 spinners having 2 different spin frequencies (*Materials and Methods* explains how different frequencies can be generated using a rotating magnetic field). Fig. 3*F* shows that in this configuration a higher-frequency spinner ($f_s = 37$ Hz) occupies an inner orbit, while the low-frequency one ($f_s = 2.5$ Hz) orbits close to the cell edge. The orbital motion of the 2 spinners in this case is perfectly synchronized: They maintain their relative orbital phases.

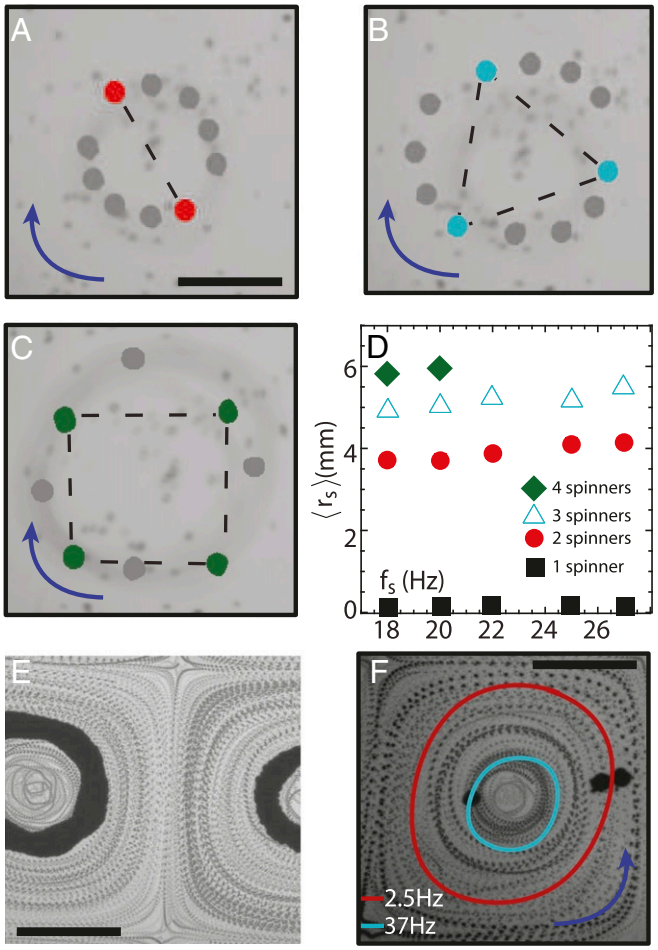

Fig. 3. Trapping of multiple spinners. (*A–C*) Confinement of multiple spinners within a unit cell. The wave frequency is 9.4 Hz and the wave's amplitude is 0.4 mm (Movies S2–S4). (*D*) Radii of the spinner orbits as a function of the spinners' frequency. (*E*) Trajectories of 2 oppositely rotating spinners of the same frequency ($f_s > 10$ Hz) trapped within 2 adjacent unit cells (average over 60 orbit periods). Gray lines show trajectories of the tracer particles. The separatrix between the unit cells is not perturbed by the presence of the spinners. (*F*) Two corotating spinners with the spin frequencies of $f_s = 2.5$ Hz (red trajectory) and $f_s = 37$ Hz (light blue trajectory) occupy different orbits. Azimuthal orbiting of the spinners is perfectly synchronized in time. (All scale bars, 4.5 mm.)

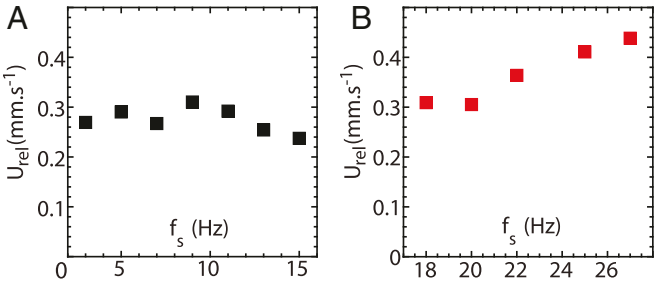

Fig. 4. Azimuthal velocity relative to the fluid drift velocity of (*A*) a single spinner (black squares) and (*B*) 2 spinners orbiting around the cell center (red squares).

Discussion

The existence of stable orbits for a single spinner within a wave-sustained unit cell is possible if the centrifugal force acting on a passive inertial particle is balanced by the inward force acting on the spinner. The most likely candidate for such a force is the lift or the Magnus force acting on a spinning particle (27, 29), which we estimate as $\vec{F}_M \simeq \rho r_0^2 h_0 \left[\vec{f}_s \times \vec{V}_{rel}\right]$, where ρ is the fluid density, r_0 and h_0 are the radius and the height of the spinning disk, and V_{rel} is the velocity of the spinner relative to the fluid. If this velocity is in the direction of the background flow V_θ, then for a corotating spinner the Magnus force should be radially inward. A change in the direction of the spinner rotation causes the reversal of the Magnus force and the spinner is pushed out into an adjacent cell. The existence of the relative spinner–fluid velocity agrees with Fig. 1*B*. This velocity seems to be independent of the spinner frequency (Fig. 4*A*). This means that the Magnus force acting on a single spinner is proportional to $\vec{f}_s$. Thus, either the inward-directed Magnus force balances the centrifugal force due to the motion of the inertial particle (spinner) along the curvilinear trajectory or the Magnus force dominates when the spinner is trapped near the cell center.

The nature of the single-spinner propulsion is not quite clear. We performed experiments on the surface of a still fluid and found no such propulsion if a single spinner is placed away from the walls of the container. The possible reason for the relative motion of the spinner is the presence of the radial gradient of the azimuthal velocity of the wave-driven drift $(\partial V_\theta/\partial r)$. It is well known that a solid particle in a viscous fluid (at zero Reynolds number) will experience a force due to a nonuniform ambient flow. For example, a sphere of radius r_0 will acquire both translational and rotational corrections, known as the Faxen law corrections, which are proportional to the Laplacian of the ambient flow velocity (28, 30). The translational velocity is given by $\vec{V}_t = \left[\left(1 + (r_0^2/6)\nabla^2\right)\vec{V}\right]$ measured at the center of a spinner (28, 30), where $\vec{V}$ is the velocity of the ambient flow without a spinner. The dominant ambient flow for the spinners within liquid metamaterials is the azimuthal drift of fluid in a unit cell (Fig. 1*B*). An azimuthal projection of a 2D Laplacian in the polar coordinates of such a flow is given by $(\nabla^2 V)_\theta = (\partial^2 V_\theta/\partial r^2) + (1/r^2)(\partial^2 V_\theta/\partial\theta^2) + (1/r)(\partial V_\theta/\partial r) - V_\theta/r^2$. Since in the inner two-thirds of a unit cell radius fluid rotates as a solid body, the translational velocity of a disk in the θ direction will be dominated by the radial gradient of the azimuthal fluid velocity: $V_t^\theta \propto (1/r)(\partial V_\theta/\partial r)$. Indeed, our results show that the Magnus force is proportionate to $(\partial V_\theta/\partial r)$. We also observe higher self-propulsion velocities of the spinners within a metamaterial cell for larger disks (1- and 2-mm diameter disks have been compared).

Then if $V_{rel} \propto (\partial V_\theta/\partial r)$, the Magnus force should be dependent on the wave amplitude A_w. It was shown that in the liquid

metamaterial, azimuthal drift velocity $V_\theta \propto A_w^{1.5}$ (figure 9 in ref. 24). Then the Magnus force $F_M \propto V_{rel} \propto (\partial V_\theta/\partial r) \propto A_w^{1.5}$, while the centrifugal force scales as $F_c \propto V_\theta^2 \propto A_w^3$. This explains why the spinner is pushed out by the centrifugal force as the wave amplitude is increased (Fig. 2*F*): The centrifugal force scales as A_w^3, while the Magnus force scales as $A_w^{1.5}$.

To test the role of the shear of the azimuthal velocity $(\partial V_\theta/\partial r)$ in the generation of the spinner propulsion and the associated Magnus force, we perform additional experiments using a flow in which spinners are drawn toward the center of a potential well. In this case an outward-directed Magnus force can be used to control the spinner orbit. We perform experiments in a flow produced in a cylindrical container whose bottom rotates relative to the walls (Fig. 5*A*). The momentum is transferred into the fluid from the rotating bottom while the walls ensure zero azimuthal velocity at the edge. Such a flow develops a radial profile of the azimuthal velocity at the fluid surface (Fig. 5*B*) which is similar to that within a unit cell of the wave-driven metamaterials (Fig. 1*B*). The rotating flow resembles a 3D von Kármán flow (31): Fluid on the surface is drawn toward the center of the cylinder such that the return flow forms in the bulk of the liquid. The central core (inner 5- to 6-mm radius) is essentially a sink, while the outer region is suitable for testing interactions between the flow gradient and a spinning disk. In contrast to the wave-driven vortex, where a surface inertial particle is pushed out from the vortex center by the centrifugal force, in the von Kármán flows floating particles are pushed inward (while executing azimuthal orbiting). This results in the passive particle following the inward spiral trajectory shown in Fig. 5*C*. After being accelerated inward from the edge, the particle slows down radially and then slowly drifts toward the vortex center. To generate stable particle orbits, the Magnus force needs to be directed outward. Indeed, when we make the spinner rotation opposite to the rotation of the vortex, the particle is pushed out of the region of positive $(\partial V_\theta/\partial r)$. By adjusting the spinner frequency, one can precisely control the orbit radius, as seen in Fig. 5*D*. In the von Kármán flow experiment, the increase in f_s pushes the spinner orbit toward the wall. It is interesting to note that even when f_s is high, the spinner never hits the wall of the container. This is because the velocity gradient $(\partial V_\theta/\partial r)$ changes sign near the wall, and the direction of the Magnus force reverses. In the liquid metamaterials, such a reversal of $(\partial V_\theta/\partial r)$ and of the Magnus force occurs at the separatrix between 2 adjacent cells.

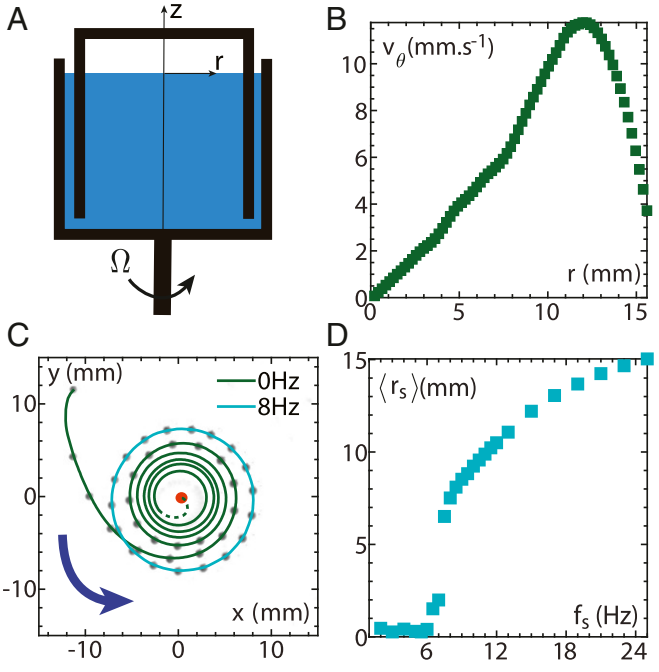

Fig. 5. Model experiment in rotating flow. (*A*) Schematic of the experiment. (*B*) Radial profile of the azimuthal velocity of the tracer particles. (*C*) Trajectories of a passive disk (green squares) and of the spinner at $f_s = 8$ Hz rotating in the direction opposite to the fluid rotation (light blue). The red disk at the center of the container represents the final stage (trapped disk) of the green trajectory. (*D*) Radii of the stationary orbits of the counter-rotating spinner (light blue squares) versus the spinner frequency f_s. The radius of the stationary cylindrical wall is 20 mm.

Let us now discuss the confinement of multiple spinners. The repulsive force between 2 spinners in the fluid at rest was studied theoretically and experimentally in refs. 1, 3, and 32. The force is quadratic in frequency: $F_{rep} \propto f_s^2$. Even in the absence of the background flow, clusters of corotating spinners move along a circular path in a horizontal plane, as discussed in ref. 32. The precession of the cluster attests to its ability to move relative to the fluid due to the spinner–spinner interaction. Two, 3, and 4 spinners orbiting in synchrony enhance their velocity relative to the fluid, which is proportional to $f_s V_\theta$. This is consistent with the observation in Fig. 3*D* which shows that in contrast to the single spinner (whose propulsion is independent of f_s; Fig. 4*A*), the rotation of a pair of spinners is increased with the increase in f_s (Fig. 4*B*). Then the Magnus force should be proportional to $f_s^2 V_\theta$ which represents the collective effect. We thus have the repelling force between 2 corotating spinners proportional to f_s^2, while the confining Magnus force has 2 parts: one proportional to $V_\theta f_s$ (acting on a single spinner) and another one proportional to $f_s^2 V_\theta$ due to the spinners' interaction. This would make the orbit radius weakly dependent on f_s as indeed is seen in Fig. 3*D*.

Full understanding of the forces acting on rotating particles in flows is a challenging problem, mainly because most effects correspond to the particle Reynolds number of order unity or higher. The problem deserves future studies going well beyond this work. In particular, it is important to better understand the mechanism of the spinner propulsion relative to the fluid in the presence of sheared flows. It should be noted that active microswimmers, such as those equipped with flagella, have actuation mechanisms different from those of the externally powered spinners studied here (28). This affects the dynamics of the swimmers in vortical lows: Self-propelled particles can move away from the center of rotation (33, 34) while in the reported experiments the radial Magnus force pushes spinners toward the center of the unit cell.

Summarizing, the wave-driven vortex lattice shows an efficient and robust way of controlling trapping of the spinning particles. The Magnus force can be manipulated to balance other radial forces in the flow to precisely control the radius of the orbit and the selection of the trapping unit cell. Liquid metamaterials are capable of trapping multiple self-assembled spinners either within a single unit cell or in the separate unit cells. Note that the main difference between the experiment performed in ref. 1 and our experiment is related to the nature of the confinement potential. In ref. 1, magnetic rotors are confined using a magnetic well. Here the hydrodynamic coupling between the spinners and the flow in the liquid metamaterials is responsible for the particle confinement.

The results offer a powerful tool which can be used in different scientific and engineering contexts. In particular, adjacent unit cells of liquid metamaterials can confine different chemical or living cell populations, while spinners can be "mules," carrying biological and chemical agents back and forth inside the cell and between the cells.

Materials and Methods

Waves. To generate stable reproducible standing waves, printed paddles (PLA Ultimaker) are mounted on 4 separate electrodynamic shakers

(TiraVibTV 5009). The 4 paddles form a square cavity 50×50 mm^2. The opposite paddles move synchronously, in phase. Two orthogonal pairs of wavemakers are time phase shifted by $\pi/2$ using a waveform generator (Keysight 33500B Series). In all of the experiments, the paddle oscillation frequency is fixed at 9.4 Hz to fit integer number of wavelengths within the square cavity. The container depth is $h = 15$ mm, ensuring the deep water wave approximation. The wave dispersion relation is given by $\omega^2 = gk + \gamma/\rho k^3$, where g is the acceleration of gravity and γ is the liquid surface tension.

Magnetic Field. Two sets of Helmholtz coil pairs powered by 2 waveform amplifiers (Accel Instruments TS250-0) create a rotating magnetic field at the surface of the liquid. Sinusoidal magnetic fields generated by each pair of coils are phase shifted by $\pi/2$, creating the field rotating at the frequency f_s. The rotation direction is reversed by changing the phase between the magnetic coil pairs from $\pi/2$ to $-\pi/2$.

Flow Measurements. The horizontal fluid flow is visualized using buoyant tracer particles (polyethylene, specific density 1.006 g/cm^3, 53 to 63 μm, microspheric). The Stokes number is given by $St = (2/9)(\rho_p/\rho_f)(d_0/L_f)^2 Re$, where ρ_p and ρ_f are respectively the densities of the particles and of the fluid. L_f is the characteristic scale of the flow, for example the radius of the fluid particle gyro-orbit (about 0.5 mm here). For the tracer particles at typical Reynolds numbers of $Re = 10$, the Stokes number is $St = 2.10^{-2}$ suggesting that their finite size should not lead to the deviation of their trajectories from those of the fluid particles. A high-resolution video camera (Andor Zyla X5.5; 2,560 $\times$ 2,160 pixels, 100 fps) is used to record the motion of the tracer particles.

Spinners. Ferromagnetic spinners (1-mm diameter) are made using a flexible 3D printed (PLAflex) template patterned with cylindrical holes. The holes are loaded with a mixture of polymers (Elite Double 8) and nickel powder ($<$150 μm; Sigma Aldrich), where the nickel powder constitutes 90% of the mixture mass. To ensure that the spinner magnetization is diametrical, the 3D printed template containing the spinners is exposed for 3 d to a strong horizontal and uniform magnetic field of 2 T. When placed on the water surface, the spinners are energized using a rotating magnetic field. The spinner rotation frequency f_s is checked using a high-speed camera. The Stokes number for the nonrotating spinners is $St = 10$. Their density is higher than the water density (specific gravity 1.06). The finite size of the spinners and their higher density are responsible for the inertial forces discussed above.

The spinners are magnetized particles that attract each other. At the distances between the spinner centers of about 1 to 2 mm (corresponding to (2 to 4)r_0), the hydrodynamic repulsion balances the magnetic attraction and the spinners form stably rotating pairs, as illustrated in Movie S5. The magnetic attraction force between 2 magnetic dipoles scales with the distance r between them as $1/r^4$ or even faster for rotating dipoles. The hydrodynamic repulsion force, on the other hand, scales as $1/r^3$ (1, 32). When 2 spinners are separated by a long distance (typically $>$4 to 5 times their size), the hydrodynamic repulsion dominates over the magnetic attraction. The stable rotating pair of spinners is observed at the distance between them at which magnetic attraction balances hydrodynamic repulsion. In this paper, at the separation distances larger than 3 to 4 mm hydrodynamic forces dominate and magnetic attraction can be neglected.

One can also create a configuration where rotating disks acquire different spin frequencies. When the spinner frequency exceeds some critical value (typically above 35 Hz), it may eventually stop spinning in the rotating magnetic field. We use this to create spinner configurations with different rotation frequencies. Since 2 spinners are not ideally the same, we adjust the spinner frequency near the critical value at which 1 of the 2 spinners stops rotating. The repulsion hydrodynamic force between them ceases, and magnetic interaction will attract the 2 disks forming a bigger structure, as seen in Fig. 3*F*. The double spinner rotates with much smaller frequency of 2.5 Hz in the example in Fig. 3*F*.

Data Availability

All data are available in the main text, *SI Appendix*, or on Figshare (data used for Fig. 2B: https://figshare.com/s/6d92ceab338607923f1e; custom Matlab code: https://figshare.com/s/641b204f501f0b8c5c16).

ACKNOWLEDGMENTS. This work was supported by the Australian Research Council Discovery Projects and Linkage Projects funding schemes (DP160100863, DP190100406, and LP160100477). H.X. acknowledges support from the Australian Research Council Future Fellowship (FT140100067). N.F. acknowledges support by the Australian Research Council's Discovery Early Career Research Award (DE160100742). G.F. acknowledges support by the Minerva, Simons, Israeli, and Binational Science foundations.

1. B. A. Grzybowski, H. A. Stone, G. M. Whitesides, Dynamic self-assembly of magnetized, millimetre-sized objects rotating at a liquid–air interface. *Nature* **405**, 1033–1036 (2000).
2. B. A. Grzybowski, X. Jiang, H. A. Stone, G. M. Whitesides, Dynamic, self-assembled aggregates of magnetized, millimeter-sized objects rotating at the liquid-air interface: Macroscopic, two-dimensional classical artificial atoms and molecules. *Phys. Rev. A* **64**, 011603 (2001).
3. B. A. Grzybowski, H. A. Stone, G. M. Whitesides, Dynamics of self assembly of magnetized disks rotating at the liquid-air interface. *Proc. Natl. Acad. Sci. U.S.A.* **99**, 4147–4151 (2002).
4. A. G. Marin, H. Gelderblom, D. Lohse, J. H. Snoejer, Order-to-disorder transition in ring-shaped colloidal stains. *Phys. Rev. Lett.* **107**, 085502 (2011).
5. A. Snezhko, I. S. Aranson, Magnetic manipulation of self-assembled colloidal asters. *Nat. Mater.* **10**, 698–703 (2011).
6. G. Kokot, D. Piet, G. M. Whitesides, I. S. Aranson, A. Snezhko, Emergence of reconfigurable wires and spinners via dynamic self-assembly. *Sci. Rep.* **5**, 9528 (2015).
7. G. Kokot *et al.*, Active turbulence in a gas of self-assembled spinners. *Proc. Natl. Acad. Sci. U.S.A.* **114**, 12870–12875 (2017).
8. A. Deblais, R. Harich, A. Colin, H. Kellay, Taming contact line instability for pattern formation. *Nat. Commmun.* **7**, 12458 (2016).
9. R. Grimm, M. Weidemuller, Y. B. Ovchinnikov, "Optical dipole traps for neutral atoms" in *Advances in Atomic, Molecular, and Optical Physics*, B. Bederson, H. Walther, Eds. (Elsevier, 2000), vol. 42, pp. 95–170.
10. I. Bloch, Quantum coherence and entanglement with ultracold atoms in optical lattices. *Nature* **453**, 1016–1022 (2008).
11. N. Francois, H. Xia, H. Punzmann, P. Fontana, M. Shats, Wave-based liquid-interface metamaterials. *Nat. Commmun.* **8**, 14325 (2017).
12. I. Bloch, J. Dalibard, W. Zwerger, Many-body physics with ultracold gases. *Rev. Mod. Phys.* **80**, 885–964 (2008).
13. G. Cipparrone, R. J. Hernandez, P. Pagliusi, C. Provenzano, Magnus force effect in optical manipulation. *Phys. Rev. A* **84**, 015802 (2011).
14. V. Bacot, G. Durey, A. Eddi, M. Fink, E. Fort, Phase-conjugate mirror for water waves driven by the Faraday instability. *Proc. Natl. Acad. Sci. U.S.A.* **116**, 8809–8814 (2019).
15. P. Chen *et al.*, Microscale assembly directed by liquid-based template. *Adv. Mater.* **26**, 5936–5941 (2014).
16. L. Domino, M. Tarpin, S. Patinet, A. Eddi, Faraday wave lattice as an elastic metamaterial. *Phys. Rev. E* **93**, 050202 (2016).
17. D. Nishiguchi, I. S. Aranson, A. Snezhko, A. Sokolov, Engineering bacterial vortex lattice via direct laser lithography. *Nat. Commun.* **9**, 4486 (2018).
18. Y. Sumino *et al.*, Large-scale vortex lattice emerging from collectively moving microtubules. *Nature* **483**, 448–452 (2012).
19. I. H. Riedel, K. Kruse, J. Howard, A self-organized vortex array of hydrodynamically entrained sperm cells. *Science* **309**, 300–303 (2005).
20. J. Sommeria, Experimental study of the two-dimensional inverse energy cascade in a square box. *J. Fluid Mech.* **170**, 139–168 (1986).
21. J. Paret, P. Tabeling, Experimental observation of the two-dimensional inverse energy cascade. *Phys. Rev. Lett.* **79**, 4162–4165 (1997).
22. H. Xia, M. Shats, G. Falkovich, Spectrally condensed turbulence in thin layers. *Phys. Fluids* **21**, 125101 (2009).
23. G. Stokes, On the theory of oscillatory waves. *Trans. Camb. Philos. Soc.* **8**, 441 (1847).
24. H. Xia, N. Francois, J. B. Gorce, H. Punzmann, M. Shats, Generation of vortex lattices at the liquid-gas interface using rotating surface waves. *Fluids* **4**, 74 (2019).
25. N. Francois, H. Xia, H. Punzmann, M. Shats, Inverse energy cascade and emergence of large coherent vortices in turbulence driven by Faraday waves. *Phys. Rev. Lett.* **110**, 194501 (2013).
26. N. Francois, H. Xia, H. Punzmann, S. Ramsden, M. Shats, Three-dimensional fluid motion in Faraday waves: Creation of vorticity and generation of two-dimensional turbulence. *Phys. Rev. X* **4**, 021021 (2014).
27. G. Falkovich, *Fluid Mechanics* (Cambridge University Press, ed. 2, 2018).
28. Y. Fily, A. Baskaran, M. C. Marchetti, Cooperative self-propulsion of active and passive rotors, *Soft Matter* **8**, 3002 (2012).
29. S. Rubinow, J. B. Keller, The transverse force on a spinning sphere moving in a viscous fluid. *J. Fluid Mech.* **11**, 447–459 (1961).
30. C. Pozrikidis, *Introduction to Theoretical and Computational Fluid Dynamics* (Oxford University Press, ed. 2, 2011).
31. T. Von Karman, Uber laminare und turbulence reibung, *Z. Angew. Math. Mech.* **1**, 233–252 (1921).
32. E. Climent, K. Yeo, M. R. Maxey, G. E. Karniadakis, Dynamic self-assembly of spinning particles. *J. Fluids Eng.* **129**, 379–387 (2007).
33. C. Torney, Z. Neufeld, Transport and aggregation of self-propelled particles in fluid flows. *Phys. Rev. Lett.* **99**, 078101 (2007).
34. A. Sokolov, I. Aranson, Rapid expulsion of microswimmers by a vortical flow. *Nat. Commun.* **7**, 11114 (2016).